A. A. Abdel-Aziz, K. A. Mahmoud, K. M. El-Shzly, and M. F. Abd Rabbo, "Developing Heat Transfer Augmentation in a Ribbed Rectangular Duct with Different Intake Shapes", Al-Azhar University Engineering Journal, Vol.9, No.2, April 2006, 348-365.

DEVELOPING HEAT TRANSFER AUGMENTATION IN A RIBBED RECTANGULAR DUCT WITH DIFFERENT INTAKE SHAPES

Abdel-Aziz A. A.; Mahmoud K. A.; El-Shazly K. M.; Abd Rabbo M. F.
Faculty of Engineering, Shoubra, Benha University, Egypt

تم عمل محاكاة لمسلك تبريد داخلى لريشة تربينة مزود بعروق ذات نسبة ثابتة بحيث أن عرض المسلك يبلغ أربعة أمثال ارتفاعه أى أن نسبة عرض المسلك إلى ارتفاع المسلك 4:1 لثلاثة أشكال مختلفة للمدخل وتشمل صندوق تجميع ، حافة حادة الجوانب ، و مدخل ذو شكل فوهة الجرس ، وذلك لدراسة تحسين معامل انتقال الحرارة لخصائص السريان عند منطقة الدخول لهذا المسلك بما نعطى تغير رقم رينولدز فى الفترة من 16200 إلى 72000 ونسبة ارتفاع العرق إلى القطر الهيدروليكى المكافئ 0.081 ، ونسبة خطوة العرق إلى ارتفاعه 10 و 20 . نسبة طول المسلك إلى القطر المكافئ حوالى 18.75 . وجد أن نسبة معامل ناسلت فى حالة مدخل ذو صندوق تجميع ومدخل حاد تكون أكبر من نظيرتها لمدخل ذو فوهة جرس ، ويظهر هذا التأثير بقوة عند نسبة طول خطوة للعرق 20 إذا ما قورن بنسبة خطوة 10 .

ABSTRACT

The present study is concerned with the flow and heat transfer for turbulent flow in the developing region for ribbed duct The study is based on both experimental and numerical simulations of intercooling passages of blade turbine with three different intake shapes. The effects of the different investigated parameters (Reynolds number, rib pitch, and intake shape) on the friction factor, local temperature, and local heat transfer coefficient are studied. A commercial ANSYS code [1] based on a finite element technique is used to support the experimental results. The experiments are carried out by using a wind tunnel with a suction blower and a roughened rectangular duct. It was found that the Nusselt number ratio was larger for abrupt and plenum box compared with that for bellmouth near the contraction inlet. This is due to the effect of the high turbulence at the sudden contraction inlet. The effect of intake shape on heat transfer coefficient for ribbed duct was significant for the case of rib pitch to height ratio of 20 more than that in the case of 10. Correlations were obtained for the average Nusselt number ratio in the developing region of the test duct for different intake shapes.

KEYWORDS: Entrance region, Intake shape, Ribbed duct, Fluid flow, Flow visualization, CFD Code.

1. INTRODUCTION

The effect of rough surface on the fluid dynamics and heat transfer in turbulent flow has been intensively studied over the last few years. This is due to the importance of these studies in design of turbine blades cooling passage; gas cooled reactors, and also compact heat exchangers. In all these applications the heat transfer exchanging length (typically $L/D_e = 10 - 15$) is relatively short so that the developing length (hydraulic and thermal) has a strong effect on the overall heat transfer coefficient. Therefore, the present work is directed to study the heat transfer and fluid flow characteristics through the entrance length of roughened ducts. The effect of different parameters on the heat transfer neglecting the effect of the entrance shape was extensively investigated by many of the previous investigations. Therefore, the present work is directed to study the effect of different entrance shapes on the heat transfer and characteristics for bellmouth (smooth intake), plenum box, and abrupt intakes. In the developing length, developing heat transfer and flow friction in ribbed rectangular ducts with flow separation at inlet were investigated experimentally by Liou and Hwang [2]. The used entrance shape was an abrupt contracting entrance rectangular duct with two opposite ribbed-walls. The effect of entrance shape on a smooth tube entrance is well designed by Kays and Crawfold [3] as a nozzle entrance so that the velocity profile is close to uniform at the tube entrance. Jonathan [4] examined latticwork cooling under rotational condition with film-coolant extraction to confirm if rotation adversely affects the leading surface heat transfer as in conventionally turbulent passages. He found that the centrifugal-buoyancy forces significantly affect the flow characteristics through smooth and ribbed passages. The developing heat transfer in a duct with a detached rib array using a laser holographic interferometer technique was investigated by Liou and Wang [5]. One of the purposes of this work [5] is to examine whether the proposed detached ribs can effectively eliminate the hot spots or not. Numerical analysis of mixed convection at the entrance region of rectangular duct heated from below was carried out by Narusawa [6]. An entrance region of rectangular duct is examined numerically for a thermally developing flow between a cooled top and a heated bottom boundary, the Nusselt number takes a minimum before increases as the buoyancy-induced flow becomes dominant. Results on the effects of the sidewall thermal condition as well as the inlet gas temperature are also discussed in relation to thermal transport. Khan et. al., [7] investigated experimentally the forced convection heat transfer in developing region through a ribbed and smooth square duct with asymmetric heating. The bottom surface has a rib pitch to height ratio of 16. The mean temperature of air in the duct with ribbed wall (P/e=16) increases 1.81 percent over the duct having smooth wall. It is also observed that in case of the ribbed duct, the Nusselt number increases 6.24 percent over the smooth duct with 3.32 percent pressure drop. Heat transfer and friction coefficients have been measured by Jeremy and Roland [8] within a rectangular passage of aspect ratio 0.4 containing 45-degree staggered turbulators with a rib pitch to height of 10. Turbulators height to channel hydraulic diameter ratios change from 0.193 to 0.333. Nusselt number enhancements ranging from 2 to 3.5 were obtained over that of a smooth channel, with friction coefficient enhancement values relative to the smooth channel correlation from 20 to 65 (smooth surface friction factor is about 0.005). In contrast to low-blockage turbulated channels, the 45-degree turbulated Nu is found to be lower than that at 90-degree orientation. Therefore, in the present paper the effect of the different intake shapes on flow characteristics and heat transfer characteristics for the smooth and roughened rectangular duct is investigated. ANSYS FLOTRAN (Analytical system flow transfer) CFD (2001) [1] computational fluid dynamics code is used to determine numerically the hydrodynamic effect of entrance shape on the flow and heat transfer characteristics for forced convection through a channel with two opposite roughened walls.

2. EXPERIMENTAL SETUP

The study of the flow and heat transfer characteristics for a turbulent flow through the developing length of a roughened duct was the objective of the present work. The flow system consists of: suction air blower, flow orifice, transition duct, straightener, test section with different intake shapes. The schematic diagram of channel flow system is shown in Fig. (1). The blower was capable of providing a range of Reynolds number based on hydraulic diameter of the duct (64 mm) varies between 16,200 and 72,000. The airflow discharge is controlled at the outlet of the air blower by means of a variable outlet area (volume damper) where the air was exhausted into the atmosphere.

Test Section

The test section is 1200 mm in length and has a horizontal rectangular duct having 160 mm x 40 mm cross-section. The channel of aspect ratio 4:1 used in the present work is the same aspect ratio employed by most of the previous work Liou, [2]. Aluminum ribs with height of 5.2 mm are placed on each of the principal wall at different pitches. Construction details of the test section and the photograph of the different intake shapes are shown in Fig. (2) and Fig. (3). Pressure taps were distributed along the mid-plane of the test section. Two heating units are used to conduct heat to the top and bottom walls of test section. Each of the two heating plates is made of a highly polished aluminum plate with a main electric heater placed in close contact to it, the heater could be controlled individually by a voltage regulator to perform a constant heat flux along the entire test section. Behind the main heater asbestos insulation layers are fixed. Guard heaters are used to prevent heat losses from the backside of the main heaters. The heat flux on the heating plate is adjusted by the voltage regulator to a constant value of about 1600 W/m^2 throughout the entire course of the present measurements. Copper-Constantan thermocouples (having about 0.2 mm wire diameter) are used to measure the local wall temperature of the aluminum plate at different test locations as shown in Fig. (4). A digital indicator with an accuracy of 0.08 ºC was used to indicate the temperature. The thermocouples were calibrated by direct method and the relative error of temperature measurement is about ±0.16 %. Eighty thermocouples with a pitch of 4.5

mm distributed along a distance of 400 mm from entrance. Eight thermocouples are distributed between X/D_e =6.25 to X/D_e =12.5 and ten thermocouples are distributed between X/D_e =12.5 to X/D_e =13.28. Seven thermocouples are placed in the span-wise direction of developing length to check the two dimensionality of the flow. The junction beads of thermocouples (about 0.4 mm diameter) are cemented into small holes of 1.2mm diameters are drilled into the backside of the plate at approximately 0.5 mm from the front surface. On the backside of heating plate, 25 grooves are made of width of 3 mm and 2mm depth to house the wires of thermocouples. Two thermocouples were used to measure air temperature entering and leaving the test section. In order to find the qualitative characteristics of the flow field around the ribs, a smoke visualization technique was employed in a smoke tunnel. The smoke tunnel was used to view flow patterns, recirculation, separation, and reattachment point down-stream of the intake and around the ribs. These results of smoke tunnel were reported and discussed in Abdel Aziz [part1 [9]].

The local wall temperature (T_{wx}) along the midplane of the test plate is recorded from the output of the thermocouples. The local mean bulk temperature T_{bx} of the flow is calculated from an energy balance; $T_{bx} = T_{in} + Q_x/(mc)$. Where Q_x is the heat given to the airflow from the entrance to a certain cross section of the ribbed-duct. The heat flow is measured from electric input power to the main heater and heat losses. For each test run the electric power is about 300 Watt and the relative error of measuring is about ±1.6%. An accurate multi-meter is used in measuring for voltage and current (±0.08 volt and ±0.08 Amp.), respectively. The local heat transfer coefficient is calculated from the heat flux (q_x) from the wall to the flowing air and the difference between the local wall temperature (T_{wx}) and the local mean bulk temperature (T_{bx}); $h_x = q_x/(T_{wx}- T_{bx})$ and $Nu_x = h_x. De/k_{fx}$. Where k_{fx} is the thermal conductivity of airflow, which is calculated at local mean bulk temperature (T_{bx}). The average Nusselt number $Nu_{average}$ for the developing region from the entrance to X/D_e =6 is calculated by integrating the local Nusselt number N_{ux} over the developing length.

3. EXPERIMENTAL RESULTS

The static pressure distributions along the ribbed duct bottom wall for the developing length were measured. These results were reported and discussed by the writer earlier in part1 [9]. Experiments were carried out to study the heat transfer characteristics in the developing and fully developed regions for smooth and ribbed ducts with different rib pitches and intake shapes.

Figure (5) shows the friction factor ratio (f/f_s) versus Reynolds number in the fully developed region for roughened duct with different rib pitches and intake shapes. The friction factor ratio is independent of both the intake shape and Reynolds number for Re > 40,000. It was observed that as the Reynolds number increases, the friction factor ratio increases slowly and then it approaches to a horizontal line. For Re < 40,000 and p/e =20, the bellmouth intake have the lowest value of friction factor ratio in comparison with abrupt and plenum intakes. The local and average Nusselt numbers for the heated walls were obtained and the thermal performance characteristics were evaluated at the constraint of equal pumping power. To confirm the validity of the present measurements, a normalized Nusselt number ratio distribution of smooth duct with plenum intake versus the axial dimensionless distance are compared with Liou's data [2] as shown in Fig. (6). The present results are in good agreement with that of Liou [2]. Figures (7a, b) to (9a, b) show the dimensionless local distribution of wall temperature, and Nusselt number ratios versus the dimensionless axial distance along the roughened duct with square ribs for pitch to height ratio of P/e = 10, for different intake shapes and at different Reynolds numbers. It was observed that the trend of local temperature and Nusselt number for the different intake shapes have similar trends. The local temperature distributions were normalized with the inlet temperature (T_{in}) in the form of $(T_x-T_{bx})/T_{in}$, and the Nusselt number was normalized as a ratio of the fully developed value (Nu_x/Nu_s) in a smooth circular tube (Nu_s). It was noticed that the local temperature of roughened wall increases gradually through the thermal entry length (X/D_e=0 to 5). It was observed, that the local Nusselt ratio is higher at the leading edge of duct inlet due to the large temperature gradients near the leading edge of the duct inlet. The closed-square symbols along the abscissa of each graph in figures (7 to 10) indicate the axial position of the ribs. The local Nusselt number decreases suddenly and begins to increase again to the second sharp peak where the flow impinging the duct wall reattached at distance of about X/D_e = 0.4 and 0.5 for bellmouth and (plenum and abrupt) intakes, respectively. The Nusselt number ratio decreases gradually after the second sharp peak to the first rib due to the formation and built up of the thermal and hydrodynamic boundary layer. The local Nusselt number is then varied in a periodic manner till it approach a constant value (fully developed value) at about X/D_e = 5.0. It can concluded that two maximum peaks for the local Nusselt number were found the first at a point near the leading edge of the duct and the second around the reattachment Due to the growth of thermal boundary layer downstream of the reattachment point, the local Nusselt number decreases again to the next rib. Also, it was observed that at Reynolds numbers ranged from $1.62x10^4$ to $4.88x10^{4,}$ Nusselt number distribution is dependent on the rib pitch and intake shapes. For different intake shapes it was found that, the local Nusselt number ratio Nu_x/Nu_s for ribbed wall duct is independent of Reynolds number for $1.62x10^4<Re<4.88x10^4$, while Reynolds number affects much the temperature ratio $(T_x-T_{bx})/T_{in}$ specially for $Re<1.62x10^4$. The normalized temperature is shifted from the others that for Re = $1.62x10^4$.

Figure (10) illustrates the effect of intake shapes on the dimensionless local wall temperature and Nusselt number ratio along axial distance for roughened duct with square ribs at P/e=10 and Re $=3.68x10^4$. In the upstream portion of the first rib, the P/e ratio has a significant effect on the distributions of the local temperature ratio $(T_x-T_{bx})/T_{in}$ and Nusselt number ratio Nu_x/Nu_s that are affected by the intake shape of the duct. While in the downstream portion of the first two rib pairs, the Nu_x/Nu_s unaffected but decreases slowly and settling into a periodic pattern. Also the abrupt and plenum intakes enhance the heat transfer coefficients near the sudden contraction inlet duct with a greater extent than that for the bellmouth intake due to the high turbulence and boundary layer distortion due flow accelerate at inlet. The local Nusselt number were numerically integrated and an average values were introduced. The numerical integration was conducted at the region affected by the intake. These regions corresponding to X/D_e from 0 up to 6.16, i.e. (up to the eighth rib position for P/e=10 and up to the fourth rib position for P/e=20). Figures (11) and (12) illustrate the effect of different intake shapes (bellmouth, plenum, abrupt) on the average Nusselt number ratio $Nu_{average}/Nu_s$ at different Reynolds numbers for ribbed duct with P/e =10 and 20, respectively. It was observed that the Nusselt number ratio $Nu_{average}/Nu_s$ decreases slightly with the increase in Reynolds number for different intake shapes for square ribs. The effect of the different intake shapes were observed in the case of the abrupt and plenum intakes which have higher average Nusselt number ratio ($Nu_{average}/Nu_s$) than that for the bellmouth. For square ribs and bellmouth intake at P/e=10, the average Nusselt number ratio ($Nu_{average}/Nu_s$) was obtained within a range of 3.87 to 3.73. Also, for plenum intake it was between 3.9 and 3.81, and the value in the case of abrupt was about 3.92 to 3.82.

From the present experimental data for different intake shapes, the average Nusselt number ratio ($Nu_{average}/Nu_s$) can be correlated by the power law in terms of Re and rib pitch (p/e).

$$Nu_{average.} /Nu_s = a\, Re^{\,b}\, (p/e)^{\,c} \qquad (1)$$

$$1.62\times10^4 \le \mathrm{Re} \le 4.88\times10^4, \quad 10 \le p/e \le 20$$

The constant coefficients a,b, and c are listed below in table (1) with a maximum deviation errors of 2.1%.

Table 1. Lists the constant coefficients for equation (1)

Constants	Bellmouth	Plenum	Abrupt
.a	5.3925	5.023	4.675
.b	-0.0254	-0.0195	-0.0106
.c	-0.0383	-0.0276	-0.0350

To evaluate the performance benefits of the ribbed duct with different intakes an efficiency index at the constraints of equal pumping power was applied. Equal pumping power constraint takes into consideration the pressure drop across the heat transfer process. Therefore, the pressure drop is more significant regarding heat transfer enhancement for equal pumping power than that for equal mass flow rate. Further, by combining the experimentally determined friction factor of the enhanced configuration and those of the well-known Blasius equation for smooth duct from Liou [2] the previous equation gives a relation between the Re and Re*:

$$Re^* = f^{1/3}.\ Re.\ [0.316.\ (Re^*)^{-0.25}]^{-1/3} \qquad (2)$$

Figure (13) illustrates the effect of Reynolds number on the average Nusselt number ratio at equal pumping power constraints ($Nu_{average}/Nu_s^*$) for different intake shapes at P/e=10. It was observed that the different intake shapes have smaller effect on the ratio ($Nu_{average}/Nu_s$*) for constant pumping power than the ratio ($Nu_{average}/Nu_s$) and the heat transfer enhancement reaches about 1.85 for constant pumping.

4. COMPUTATIONAL WORK

A computation fluid dynamics (CFD) ANSYS [1] program was used to obtain the airflow pattern (velocity vectors and contours) and static pressure coefficient in the developing region of ribbed duct with different intake shapes. The program utilizes the finite element approach, which uses the k-ε turbulence model. The total number of grid elements is about 36,000 and are denser in the two dimensional plane. The Program solves the Reynolds equations, the energy equation and the equations for the turbulence energy and its dissipation.

4.1 Continuity Equation

The equation in a flow of an incompressible-fluid flow (steady or unsteady) is given by:

$$\frac{\partial u}{\partial x}+\frac{\partial v}{\partial y}+\frac{\partial w}{\partial z}=0 \qquad (3a)$$

4.2 Momentum Equation

For incompressible flow through a unit volume with no changes with time, the momentum equation in tensor form for 3-D laminar flow is given by:

$$\frac{\partial}{\partial x_i}(u_i u_j)=-\frac{1}{\rho}(\frac{\partial P}{\partial x_j})+\frac{1}{\rho}\frac{\partial}{\partial x_i}\{(\mu+\mu_t)(\frac{\partial u_i}{\partial x_j}+\frac{\partial u_j}{\partial x_i})-\frac{2}{3}\delta_{ij}k\} \qquad (3b)$$

where ρ : fluid density

P : pressure

μ : dynamic viscosity

μ_t : turbulence or eddy viscosity

x_i, x_j the coordinates

k : kinetic energy

δ_{ij} : constant=1 for i=j and = zero for i ≠j

u_i: velocity component u, v, w $(i=1,2,3)$

u_j velocity component u, v, w $(j=1,2,3)$

4.3 Energy Equation

For incompressible flow, viscous dissipation and kinetic energy are neglected. The energy equation takes an exact form which is a thermal transport equation for the static temperature as follows:

$$\frac{\partial}{\partial x}(\rho u c_p T)+\frac{\partial}{\partial y}(\rho v c_p T)+\frac{\partial}{\partial z}(\rho w c_p T)=\frac{\partial}{\partial x}(k_x\frac{\partial T}{\partial x})+\frac{\partial}{\partial y}(k_y\frac{\partial T}{\partial y})+\frac{\partial}{\partial z}(k_z\frac{\partial T}{\partial z})+Q_v \qquad (3c)$$

where c_p : specific heat of the fluid at constant pressure.

T : fluid temperature.

k : thermal conductivity.

Q_v : volumetric heat source.

All solutions apply a uniform velocity profile at inlet and zero velocity condition is applied along the walls.

Figure (14) shows the computed results obtained for roughened duct with different intake shapes. At constant Re=36,800, a comparison of flow pattern (velocity contours, vectors, and the static pressure coefficient) at developing region is given in Fig. (14). For abrupt and plenum intake shape, the flow separation point is clearly indicated at sharp inlet edge while for bellmouth intake there is no significant separation is observed. The maximum velocity vector appeared at the entrance for abrupt and plenum intakes and at the rib front edge. A clear region of vortices (circulation flow) has been created downstream the intakes of abrupt and plenum while for bellmouth there is no significant effect on the flow pattern. Negative values of static pressure coefficient (C_p) is observed nearest to the leading edge of the channel flow for plenum and abrupt intakes and also above the rib. This may be attributed to the increase of flow activity and acceleration. These values of minimum static pressure coefficient indicate that there is a greater cooling rate with the higher values of air velocity and turbulence levels.

5. CONCLUSIONS

From the experimental results for heat transfer through a sudden expansion pipe with different swirl generators techniques, it is found that the intake shapes have no significant effect on the friction factor. The plenum and abrupt intake shapes enhance the heat transfer levels and no regions with low heat transfer are observed in the corner behind the ribs. The local temperature of roughened wall increases gradually through the thermal entry length (x/D_e =0 to 5) and the local Nusselt number ratio is higher at the leading edge of duct inlet and decreases suddenly while begins to increase again to second peak where flow impinging the duct wall. The local Nusselt number ratio Nu_x/Nu_s for different intake shapes and rib pitches independent on Reynolds number within the investigated range. As the rib pitch increases the local Nusselt number ratio Nu_x/Nu_s decreases because the thermal boundary layer growth up strongly. The local Nusselt number approaches a minimum value downstream the rib directly because of the wake formation and flow separation. For square ribs and bellmouth intake at p/e=10, the average Nusselt number ratio ($Nu_{average}/Nu_s$) was obtained within a range of 3.87 to 3.73. Also, for plenum intake it was between 3.9 and 3.81, and the value in the case of abrupt was about 3.92 to 3.82. The combined effect of intake shape and rib pitch have a great effect on the heat transfer in the developing region. The effect of intake shape on heat transfer for ribbed duct is more significant with p/e = 20 than that with p/e =10. The present numerical predictions produce successfully the distribution of stream-wise velocity and static pressure coefficient close to the intake and ribbed side walls.

NOMENCLATURE

C	- specific heat of air flow, J/kg.K
C_p	- static pressure coefficient,
D_e	- equivalent hydraulic diameter, m
e.	- rib height, m
f	- average friction factor $f = \{(\Delta p/\Delta x)D_e\}/(0.5\rho u_m^2)$
f_s	- smooth circular tubes friction factor
h_x	- Local heat transfer coefficient, $W/m^2.K$
k	- thermal conductivity , W/m.K
k_{fx}	- thermal conductivity of air flow at local mean temperature, W/m.K.
L	- internal cooling passage length, m
m.	- mass flow rate of air flow, kg/s
p	- rib pitch, m
p/e	-rib pitch to height ratio (distance between successive ribs per rib height).
$\Delta p/\Delta x$	- axial pressure gradient evaluated by taking the ratio of pressure drop between two consecutive points of successive cycles to the rib pitch we take between the rib number 11,13.
q_x	- local wall heat flux, W/m^2
Q_x	- Heat given to the air from the entrance to a certain cross section.
T_{bx}	- local bulk mean air temperature, ºC
T_{in}	- inlet air temperature, ºC
T_{wx}	- local wall temperature, ºC
u_m	- axial mean velocity, m/s
X	- axial distance, m
Δx	- incremental axial distance, m
	Dimensionless Groups
Nu_x	- Local Nusselt number
Nu_s	- Nusselt number for fully developed circular smooth duct taken by M/C Adams[10]
$Nu_{average}/Nu_s$	- Average Nusselt number ratio at equal mass flow rate constraints.
$Nu_{average}/Nu_s*$	- Average Nusselt number ratio at equal pumping power constraints.
Nu_x/Nu_s	- Local Nusselt number ratio.

Re	- Reynolds number, $(\rho u D_e/\mu)$
Re*	- Reynolds number at constant pumping power.
	Greek Symbols
μ	- viscosity, kg/m.s
τ	- shear stress, kg/m.s^2
ν	- kinematics viscosity, m^2/s
ρ	- density, kg/m^3
Δ	- difference
	Subscripts
b	- bulk
d	- dynamic
e	- equivalent
in	- inlet
s	- smooth
w	- wall
x	- local distance in the axial direction of the duct at mid point span direction

REFERENCES

1. ANSYS (2001), CFD FLOTRAN Analysis Guide, ANSYS, Inc.
2. Liou, T. M., Hwang, J. J., " Developing heat transfer and friction in a ribbed rectangular duct with flow separation at inlet" Journal of Heat Transfer, Vol. 114, pp 565-573, 1992
3. Kays, W. M., and Crawfold, M. E.," Convective heat and mass transfer " 2nd ed., p.311-353 McGraw-Hill, 1980
4. Jonathan LaGrone, "Lattic work cooling with rotation and film extraction" ME graduate student conference, Vienna, April 17, 2004.
5. Liou, T. M., and Wang, W. B., " Laser holographic interferometry study of developing heat transfer in a duct with a detached rib array" Int. J. Heat and Mass Transfer, Vol. 38, No. 1, pp. 91-100, 1995
6. Narusawa, U., "Numerical analysis of mixed convection at the entrance region of rectangular duct heated from below" Int. J. Heat and Mass transfer Vol. 36, No. 9, pp. 2375-2384, 1993.
7. Khan, R. K., Ali, M A T, and Akhanda, M A R., " Comparative study on forced convection heat transfer in developing region through square ducts with a bottom ribbed and a smooth surface" IE(I) Journal-MC, Vol 84, April 2003.
8. Bailey, J. C., and Bunker, R. S., " Heat transfer and friction in channels with very high blockage 45^{o} staggered turbulators" ASME turbo Expo, June 16-19, Atlanta, Georgia, USA, 2003
9. Abdel Aziz, A.A., Mahmoud, K. A., El-Shazly, K. M., and Abd Rabbo, M. F., " Effect of different intake shapes on the fluid flow characteristics of a ribbed rectangular duct" Engineering Research Journal, Shoubra Faculty of Eng., Number 2, October 2004.
10. Ozisik, M. Necati, "Heat Transfer," McGraw-Hill, Co-singapore, 1985.

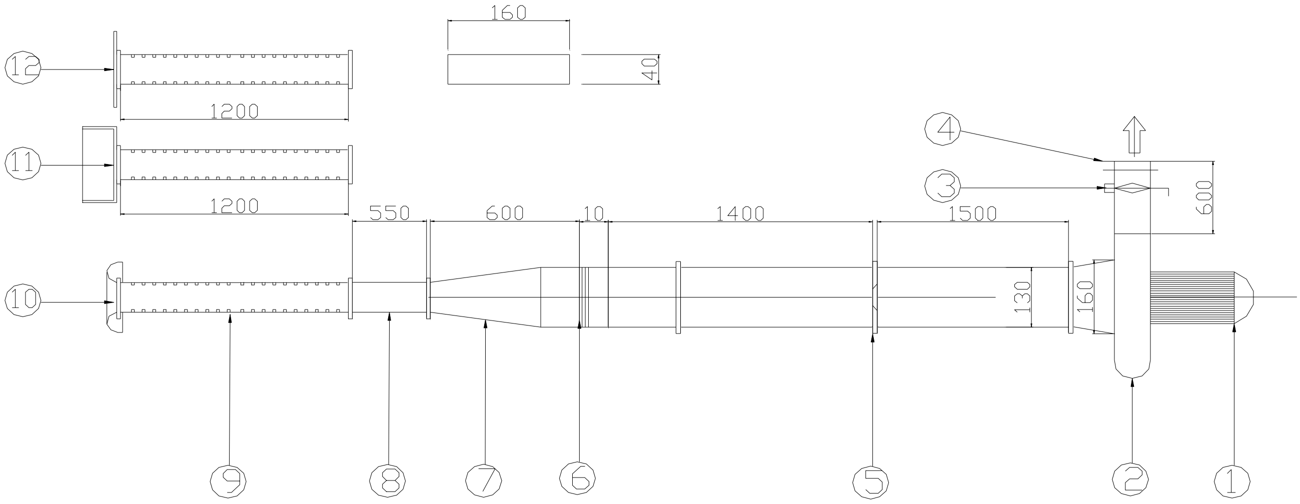

Dimensions are in mm

1. A.C electric motor 3 Hp power
2. Air blower
3. Air gate controller (Volume damper).
4. Exit duct.
5. Flow orifice meter
6. Straightener.

7- Transition duct.
8- Exit duct.
9- Test section.
10- Duct with bellmouth intake.
11- Duct with plenum intake.
12- Duct with abrupt intake.

Fig. 1. Schematic diagram of the test rig.

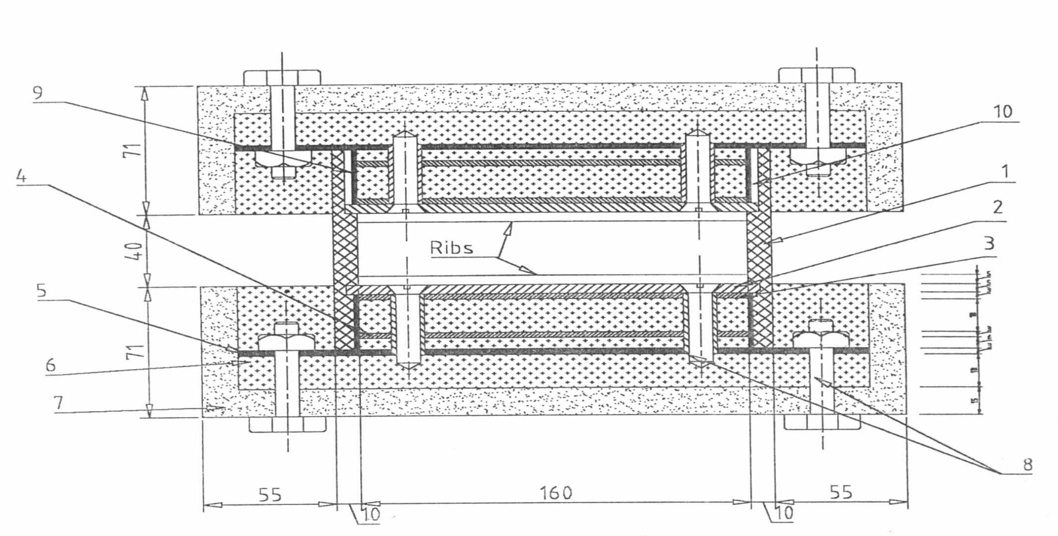

Dimensions are in mm

1.Plexiglas.
2.Aluminum plate
3.Main heater
4.Guard heater.
5.Backelite sheet.
6. Asbestos insulation
7. Wooden frame
8. Fixation and assembly.
9. Heaters edge insulation.
10. Wires gap inside the frame.

Fig. (2) Cross section detail of the test channel for heat flow measurements.

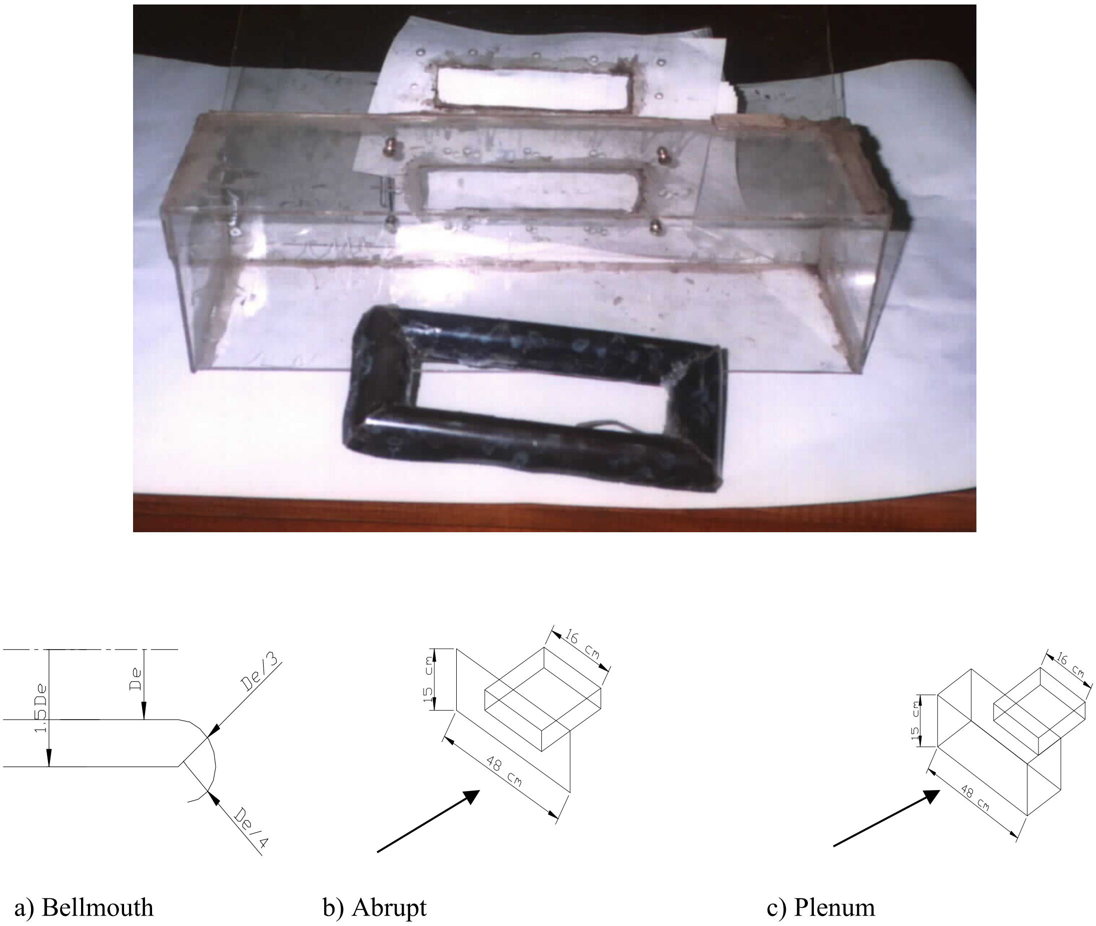

Fig. 3. Photograph and schematic diagram of the different intake shapes.

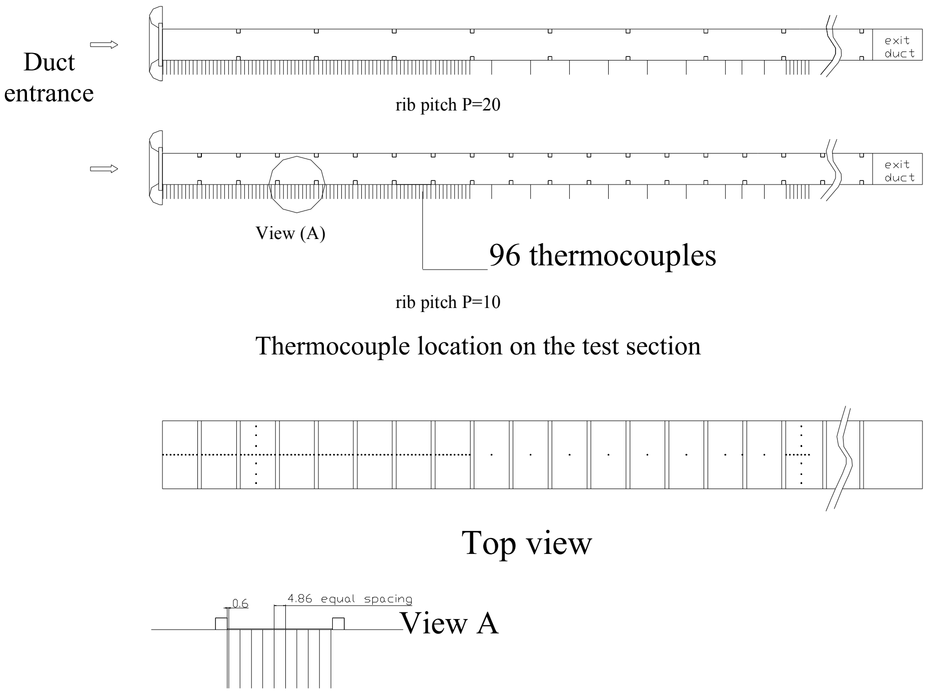

Fig. 4. Test sections details for heat transfer measurements.

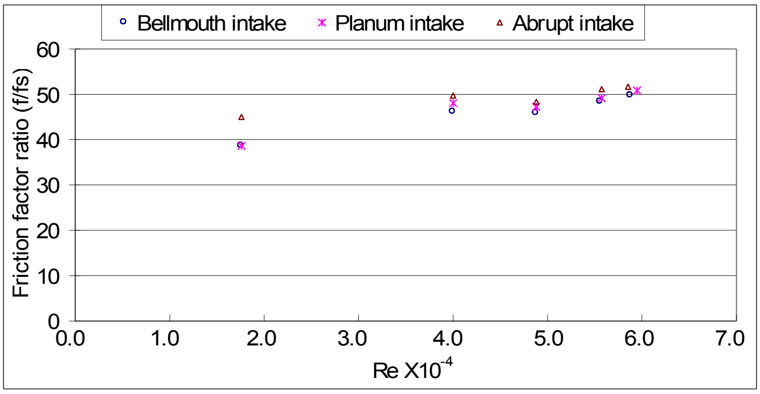

a) P/e=10

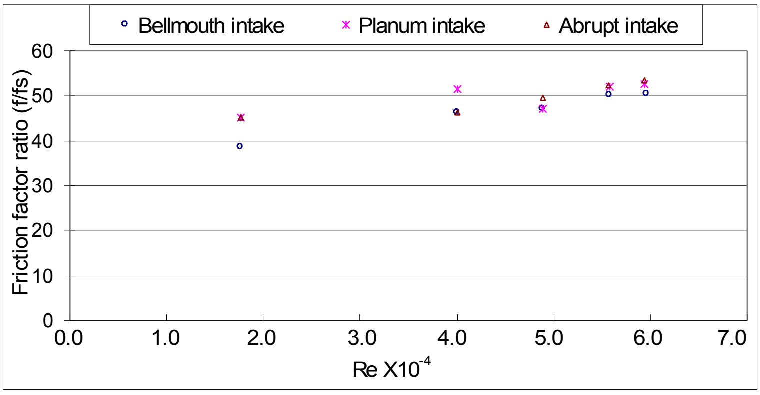

b) P/e=20

Fig.5. The fully developed friction factor ratio versus the Reynolds number for different intake shapes, for square Ribbed duct for different pitch to height ratios (p/e) of 10, 20.

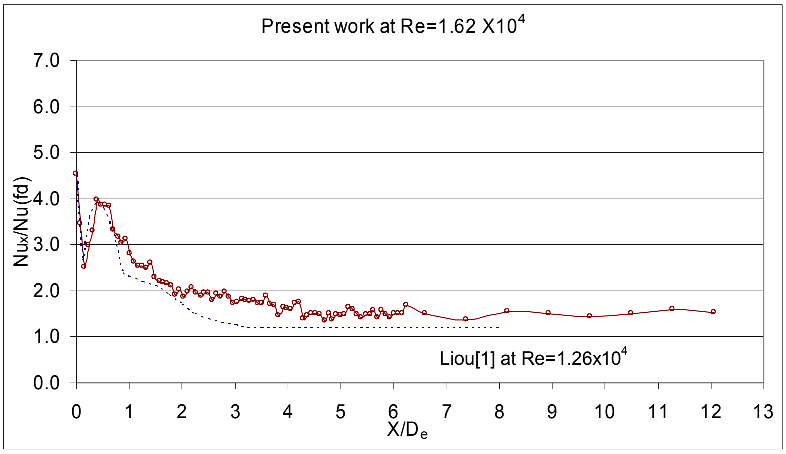

Fig. 6. Comparison between the present results and that of Liou's[2] of local Nusselt number ratio for smooth duct, for plenum intake at Reynolds number (Re=1.62 X104).

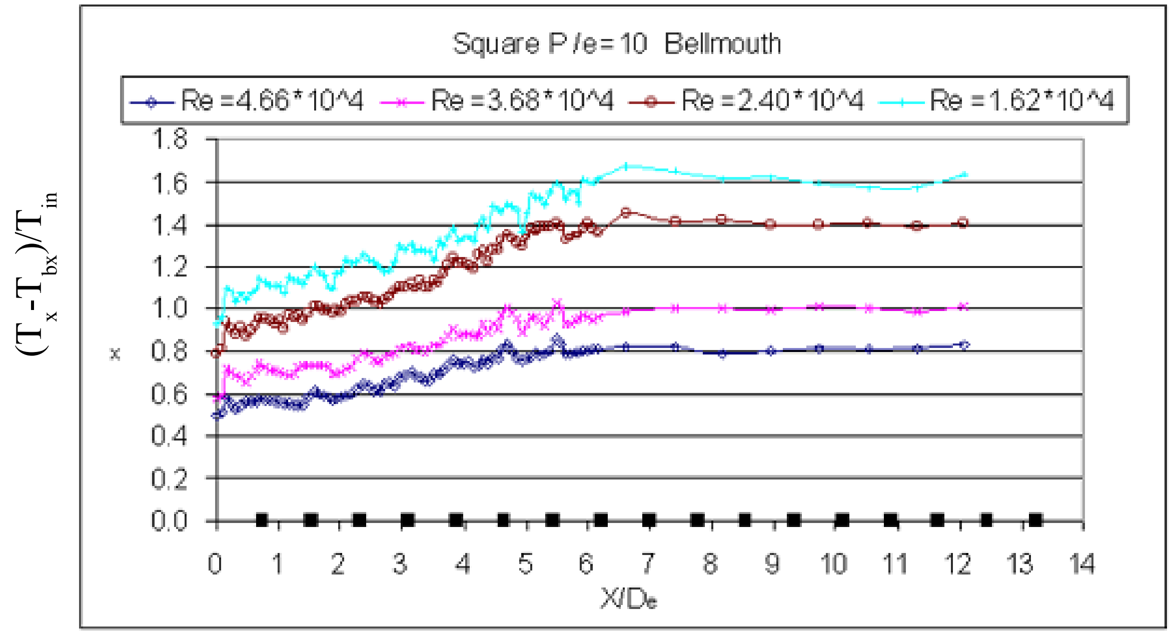

a) Normalized local wall temperature

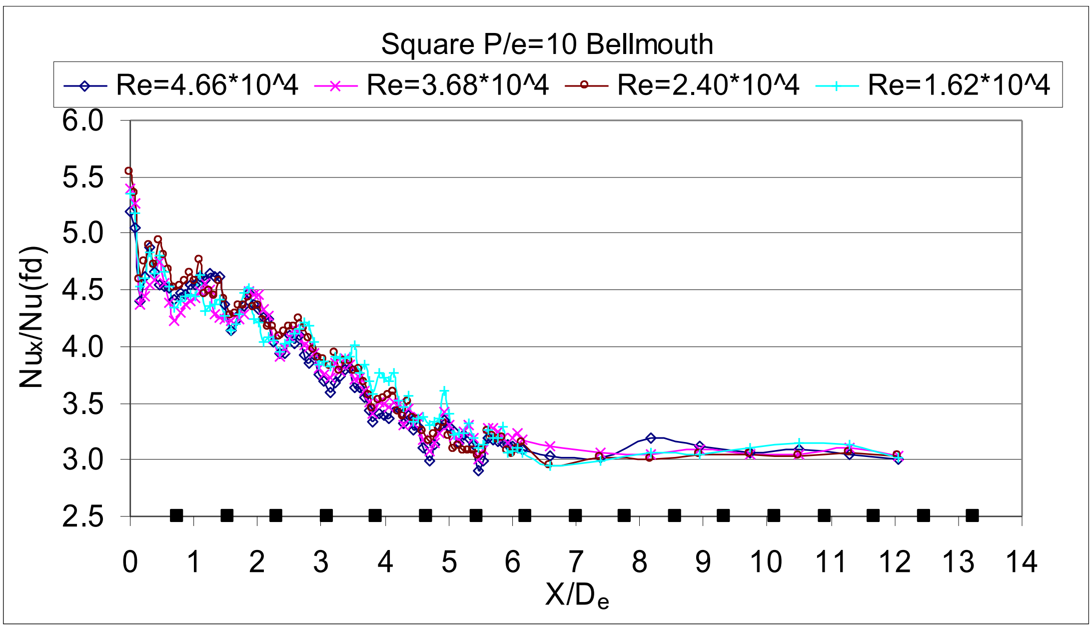

b) Normalized local Nusselt number

Fig. 7. The local Nusselt number ratio and local wall temperature ratio versus the dimensionless axial distance for ribbed duct with square ribs (p/e=10), for bellmouth intake at different Reynolds numbers.

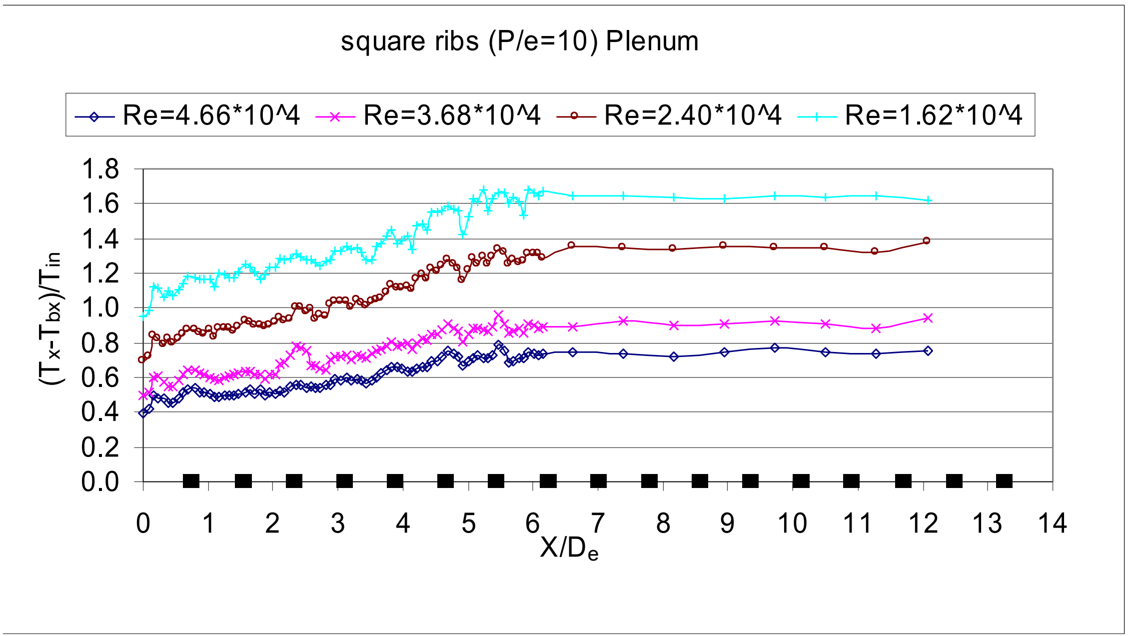

a) Normalized local wall temperature

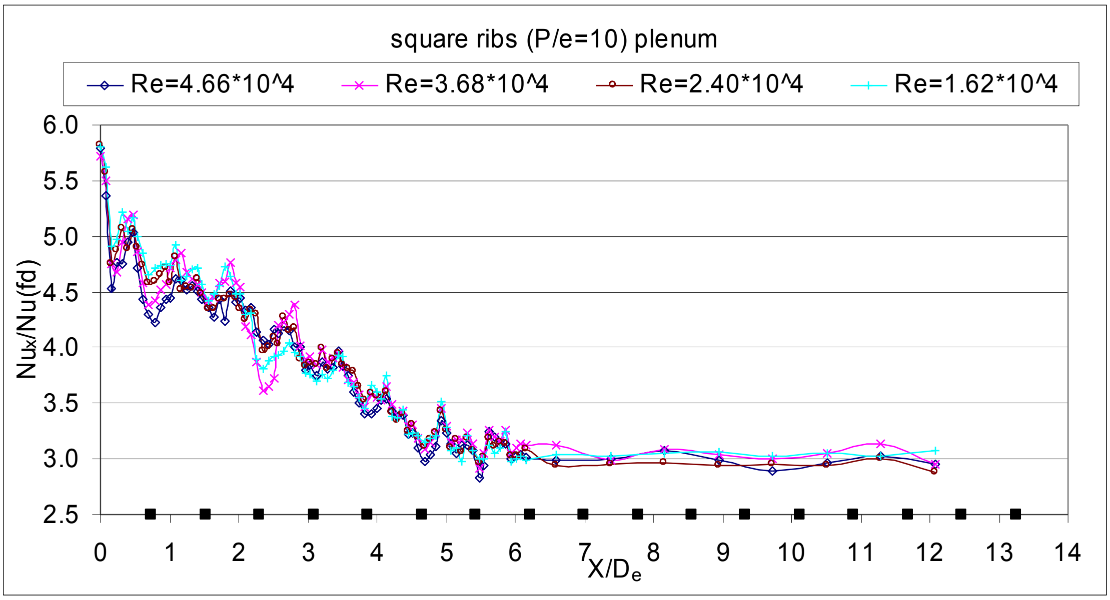

b)Normalized local Nusselt number

Fig.8. The local Nusselt number ratio and local wall temperature ratio versus the dimensionless axial distance for ribbed duct with square ribs (p/e=10), for Plenum intake at different Reynolds numbers.

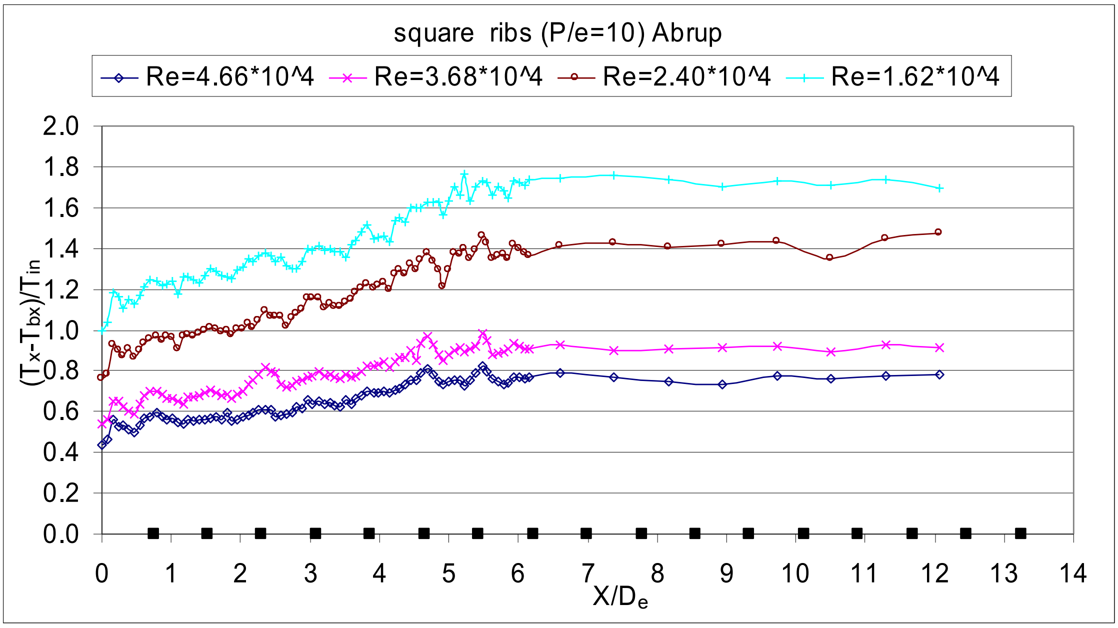

a) Normalized local wall temperature

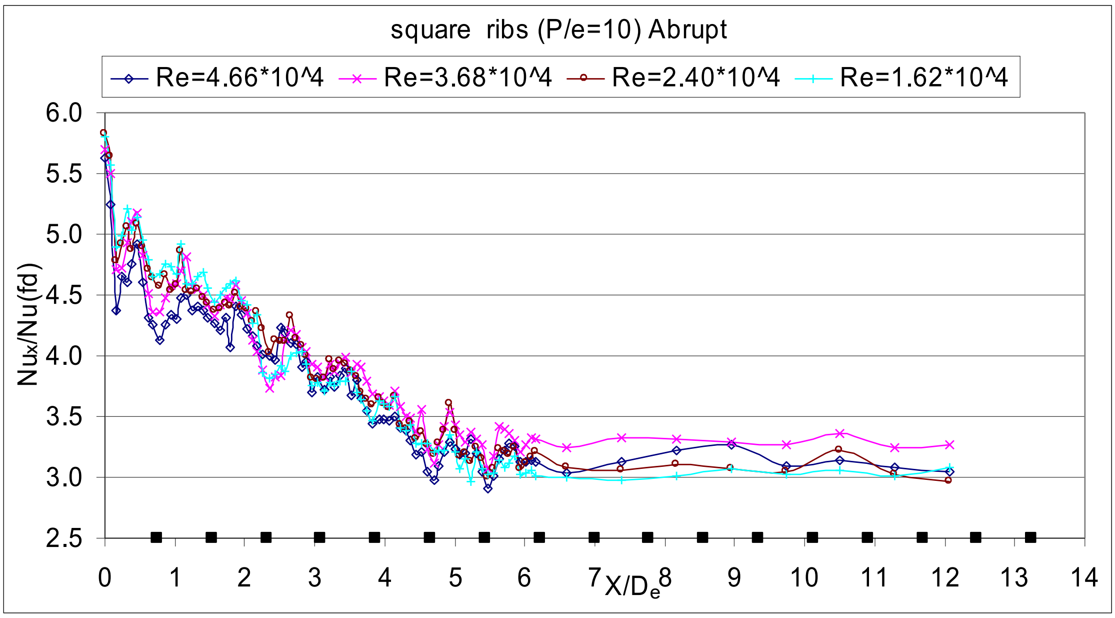

b) Normalized local Nusselt number

Fig. 9. The local Nusselt number ratio and local wall temperature ratio versus the dimensionless axial distance for ribbed duct with square ribs (p/e=10), for abrupt intake at different Reynolds numbers.

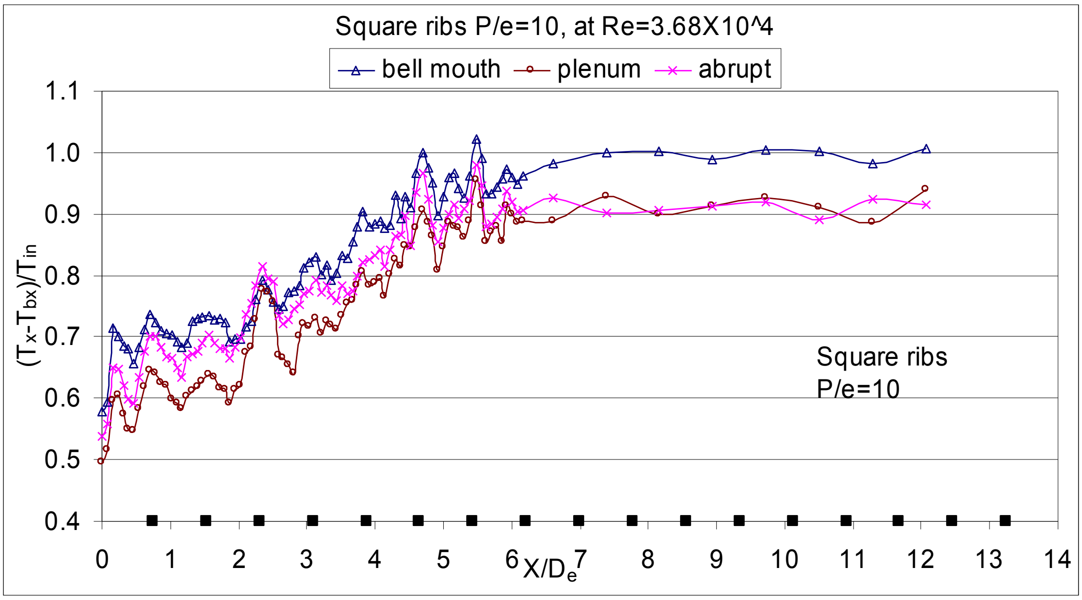

a) Normalized local wall temperature

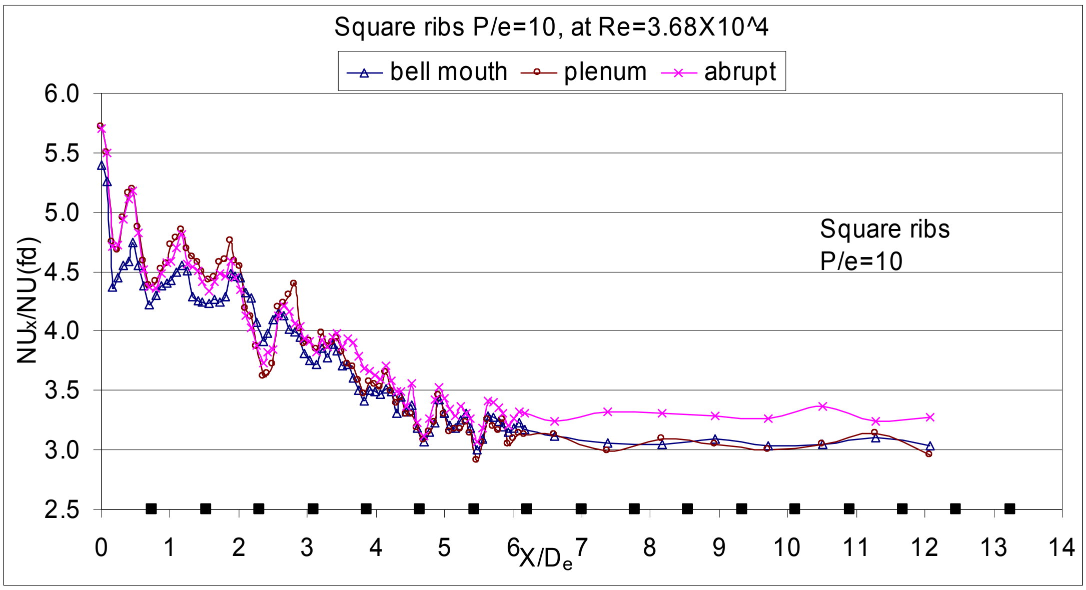

b) Normalized local Nusselt number

Fig. 10. The local Nusselt number ratio and local wall temperature ratio versus the dimensionless axial distance for ribbed duct with square ribs (p/e=10), for different intake shapes at Re=36,800 .

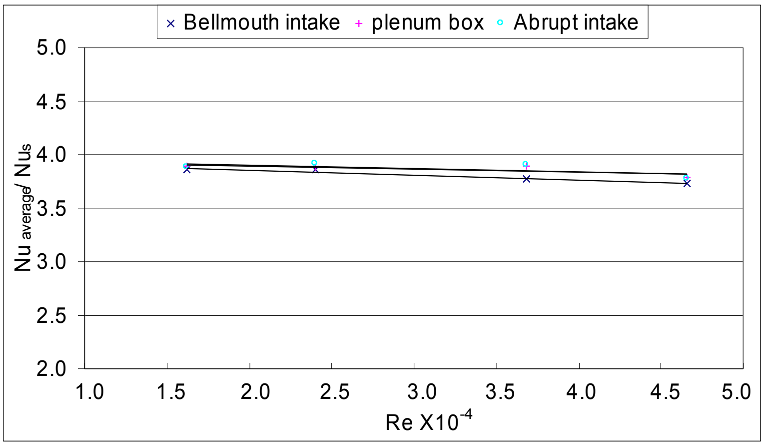

Fig. 11. Effect of the Reynolds number on the average Nusselt number ratio for square ribs at p/e = 10, for different intake shapes.

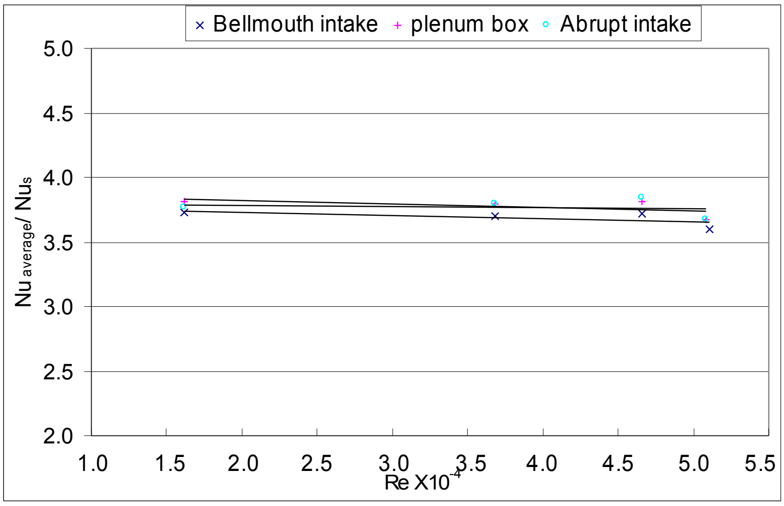

Fig. 12. Effect of the Reynolds number on the average Nusselt number ratio for square ribs at P/e = 20, for different intake shapes.

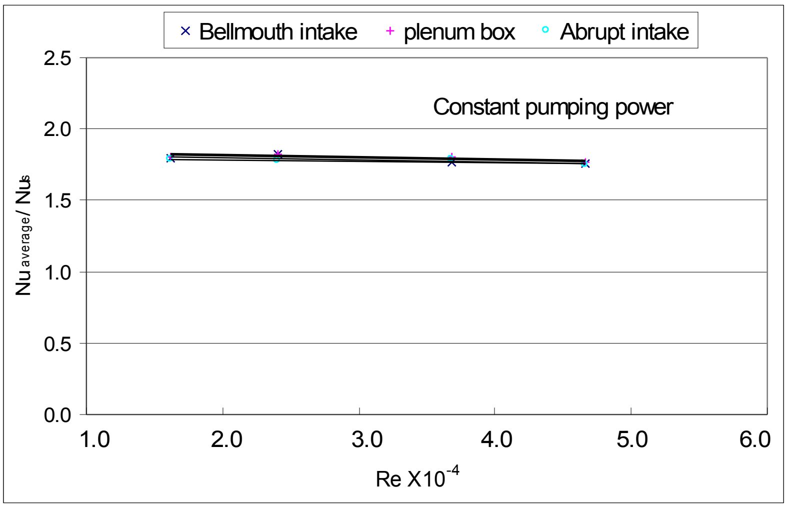

Fig.13. Effect of Reynolds number on the average Nusselt number ratio for square ribs at P/e = 10, for different intake shapes for constant pumping power constraint.

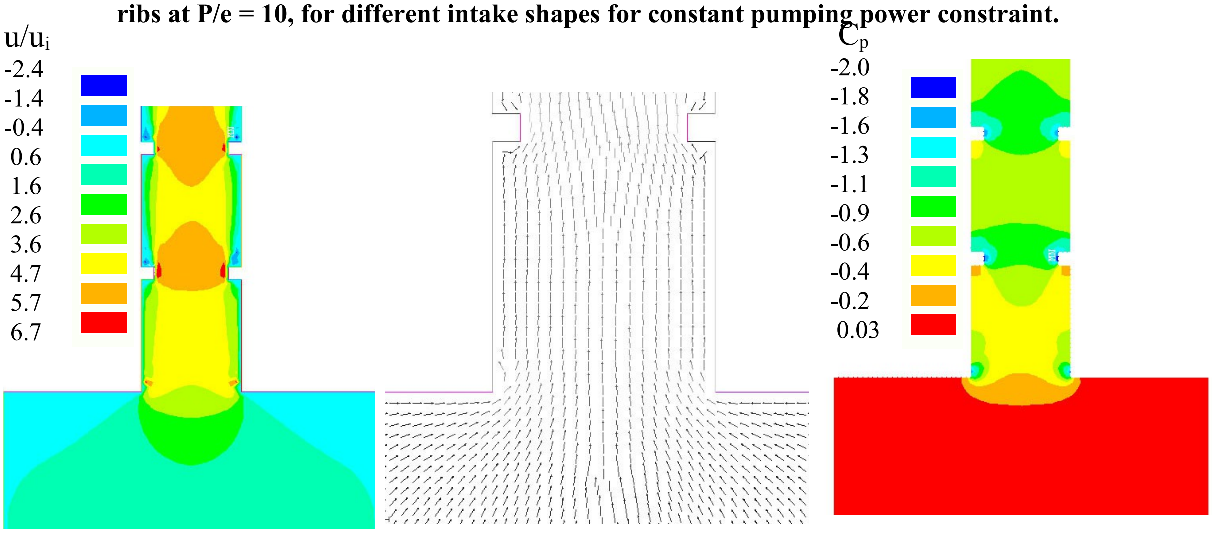

Plenum Intake

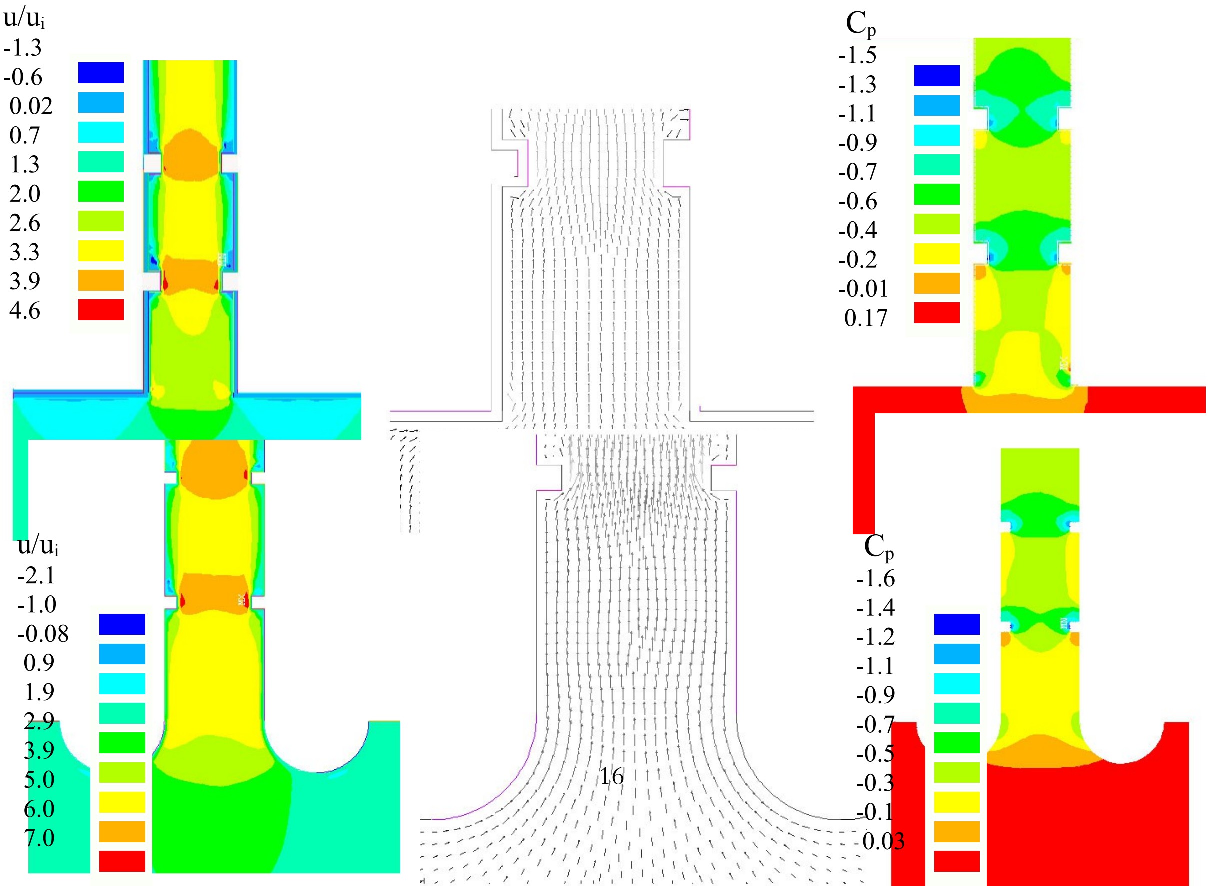

Bellmouth Intake

(a) (b) (c)

Fig. 14. Numerical predictions of flow patterns, (a) velocity contours , (b) velocity vector, and (c) pressure coefficient (c_p) contours.